Journal Pre-proof

Variations in Greenland surface melt and extreme events from 1958 to 2023

Qing-Lin ZHANG, Ming-Hu DING, Michiel R. VAN DEN BROEKE, Brice NOËL, Xavier FETTWEIS, Sai WANG, Wei-Jun SUN, Qing-Long YOU, Cun-De XIAO, Da-He QIN, Bao-Juan HUAI

PII: S1674-9278(25)00117-0

DOI: https://doi.org/10.1016/j.accre.2025.05.004

Reference: ACCRE 644

To appear in: *Advances in Climate Change Research*

Received Date: 4 March 2025

Revised Date: 17 April 2025

Accepted Date: 21 May 2025

Please cite this article as: ZHANG, Q.-L., DING, M.-H., VAN DEN BROEKE, M.R., NOËL, B., FETTWEIS, X., WANG, S., SUN, W.-J., YOU, Q.-L., XIAO, C.-D., QIN, D.-H., HUAI, B.-J., Variations in Greenland surface melt and extreme events from 1958 to 2023, *Advances in Climate Change Research*, https://doi.org/10.1016/j.accre.2025.05.004.

Variations in Greenland surface melt and extreme events from 1958 to 2023

Qing-Lin ZHANG[1,2,3], Ming-Hu DING[1,2**], Michiel R. VAN DEN BROEKE[4], Brice NOËL[5], Xavier FETTWEIS[5], Sai WANG[2], Wei-Jun SUN[3], Qing-Long YOU[1], Cun-De XIAO[6], Da-He QIN[2], Bao-Juan HUAI[3*]

1. Department of Atmospheric and Oceanic Sciences & Institute of Atmospheric Sciences & Key Laboratory of Polar Atmosphere–Ocean–Ice System for Weather and Climate, Ministry of Education, Fudan University, Shanghai 200438, China

2. State Key Laboratory of Disaster Weather Science and Technology, Chinese Academy of Meteorological Sciences, Beijing 100081, China

3. College of Geography and Environment, Shandong Normal University, Jinan 250358, China

4. Institute for Marine and Atmospheric Research, Utrecht University, Utrecht 3584, Netherlands

5. Laboratory of Climatology, Department of Geography, SPHERES research unit, University of Liège, Liège 4000, Belgium

6. State Key Laboratory of Earth Surface and Resource Ecology, Beijing Normal University, Beijing 100875, China

Correspondence to:

DING M.-H. (dingminghu@foxmail.com); State Key Laboratory of Disaster Weather Science and Technology, Chinese Academy of Meteorological Sciences, Beijing 100081, China.

HUAI B.-J. (huaibaojuan@126.com)

Abstract: Surface melt and subsequent runoff have been the main contributors to recent Greenland mass loss. However, previous studies mainly focused on the extent and persistence of surface melt. The variations in surface melt rates and extreme events have not been adequately known, especially the role of extremes in the long-term surface melt changes. Here, using two high-resolution regional climate models (RACMO2.3p2 and MARv3.14), we analyzed the variations in Greenland surface melt in 1958–2023. Both models (RACMO/MAR) show that annual surface melt is rapidly increasing post-1990 at a rate of 8.6 ± 4.9/7.2 ± 4.4 Gt per year. The northern regions show the strongest relative regional increase rate (3.9% ± 1.9%/3.4% ± 1.6% per year), contributing more surface melt to the whole Greenland. Based on the 90th percentile of the daily distribution, we found that extreme melt events from May to September (M–S) have become more frequent post–1990 (0.7/0.8 ± 0.5 d per year). Compared with 1958–1990, M–S melt from extreme events has increased by 134/105 Gt per year and dominates the increase in the total surface melt. During extreme events, we found an increase in downward longwave radiation, net shortwave radiation and sensible heat flux. The rise in surface melt and extreme events post-1990 is linked to more frequent atmospheric blocking. This study improves our understanding of the role in ice sheet mass balance played by long-term variations in ice sheet surface melt and extreme events.

Keywords: Greenland; Surface melt; Extreme events; Regional climate model

1. Introduction

Mass loss from the contiguous Greenland ice sheet (GrIS) and its peripheral glaciers and ice caps (GICs) is a major component of sea level rise (Chen et al., 2017; Frederikse et al., 2020). From 2017 to 2020, 17.7% of the global sea level rise was driven by GrIS mass loss (Otosaka et al., 2023), which resulted from increased ice discharge and decreased surface mass balance since the end of the 20th century (van den Broeke et al., 2016; Meredith et al., 2019; Choi et al., 2021). This reduction of surface mass balance dominated GrIS mass loss since 2000 and was related to amplified surface melt and subsequent runoff (van den Broeke et al., 2016; Meredith et al., 2019; IMBIE Team, 2020). Meanwhile, Greenland extreme surface melt events become more frequent (Nghiem et al., 2012; Tedesco and Fettweis, 2020; Box et al., 2022; Bonsoms et al., 2024). Given the importance of surface melt, it is essential to understand the changes in Greenland surface melt and events.

In-situ observations, satellite data and (regional) climate models are the most commonly used tools for GrIS surface melt analysis (Mernild et al., 2011; Tedesco and Fettweis, 2020; Zheng et al., 2022; van den Broeke et al., 2023). Analysis of variations in Greenland surface melt extent and duration has benefited greatly from developments in remote sensing. However, satellite products cannot directly observe surface melt rate, although recent studies used artificial intelligence to reconstruct the surface melt from satellite data (Zheng et al., 2022). Therefore, the changes in surface melt rates in Greenland have not been thoroughly investigated, especially the spatial differences. Surface energy balance models and regional climate models (RCMs) can be used to analyze spatial and temporal variability in Greenland surface melt rate (Noël et al., 2019; Wang et al., 2021; Bonsoms et al., 2024). They have the advantage of full spatial and temporal coverage and have outputs of surface melt rates before the satellite era (Noël et al., 2019; Fettweis et al., 2020; Bonsoms et al., 2024).

With global warming and Arctic amplification becoming ever more prominent (Serreze and Barry, 2011; Previdi et al., 2021), the Arctic experiences more frequent extreme climate events (Walsh et al., 2020), such as an increasing occurrence of heat waves (Dobricic et al., 2020; Overland and Wang, 2021). Greenland also experiences an increased frequency of extreme warming, rainfall and surface melt (Nghiem et al., 2012; Tedesco and Fettweis, 2020; Box et al., 2022). For instance, extensive surface melt over practically the entire sheet occurred in 2012 and 2019, and in 2021 rainfall was observed at Summit station, the highest point of the GrIS (Nghiem et al., 2012; Tedesco and Fettweis, 2020; Box et al., 2022). A recent study has projected that GrIS mass loss will rapidly increase with future extreme melt events (Beckmann and Winkelmann, 2023). However, we have not adequately known the long-term changes in extreme surface melt events and their role in the long-term increase in Greenland surface melt.

Here we used two high-resolution polar regional climate models—the Regional Atmospheric Climate Model (RACMO) version 2.3p2 and Modèle Atmosphérique Régional (MAR) version 3.14—to show the variations in Greenland surface melt and extreme events from 1958 to 2023. We linked the changes in surface melt and extreme melt events to the large-scale atmospheric circulation over Greenland and present associated anomalies of surface energy fluxes. The results will help to improve our understanding of the changes in ice sheet surface melt and extreme events and the mechanisms.

2. Material and methods

2.1 Regional climate models

We used the outputs of two high-resolution regional climate models: RACMO 2.3p2 (RACMO hereafter) and MAR v3.14 (MAR hereafter), for 1958–2023. RACMO is developed by the Royal Netherlands Meteorological Institute (KNMI) and adapted for polar glaciated regions at the Institute for Marine and Atmospheric Research, Utrecht University (IMAU/UU), specifically to simulate the climate and surface mass balance of the ice sheets of Greenland (Noël et al., 2015; Noël et al., 2018) and Antarctica (van Wessem et al., 2018). RACMO is run at 5.5 km horizontal resolution forced by ERA-40 (1958–1978), ERA-Interim (1979–1989), and ERA5 reanalysis (1990–2023). Vertically, RACMO has 40 vertical atmosphere model levels and 40 active snow layers used for simulating snow melt, water percolation and retention, refreeze and runoff (Greuell and Konzelmann, 1994; Ettema et al., 2010). In addition, RACMO also considers dry snow densification (Ligtenberg et al., 2018), and drifting snow erosion and sublimation (Lenaerts et al., 2012). The daily surface melt from RACMO is available on a horizontal resolution of 1 km, achieved by statistically downscaling the 5.5 km RACMO2.3p2 using elevation dependence and bare ice albedo correction (Noël et al., 2016; 2017; 2019). The higher-resolution grid better resolves the edge of the GrIS and GICs, especially over narrow glaciers and confined ablation zones.

The version of the hydrostatic regional climate model MAR used here is run at 10 km horizontal resolution. As a 3D atmosphere–snow model, MAR describes atmosphere dynamics (Greuell and Konzelmann, 1994) and energy and mass exchange by combining with the 1D energy balance-based snow model SISVAT (de Ridder and Gallée, 1998). MAR is coupled with the snow model CROCUS (Gallée and Duynkerke, 1997; Gallée et al., 2001; Lefebre et al., 2003). MAR here is forced at the boundaries using ERA5 during 1958–2023. MAR has improved parametric schemes of cloud and bare ice albedo and has improved dynamical stability compared to previous versions (Fettweis et al., 2020). The MAR used here was the latest version v3.14.

Sea surface temperature, sea ice cover, and lateral and top boundaries in both RCMs are prescribed from reanalysis data. Both RCMs have been extensively evaluated and proven to well represent Greenland climatology and surface mass balance (Noël et al., 2016; Fettweis et al., 2017; Noël et al.,

2019; Antwerpen et al., 2022). We also used modelled daily average surface albedo, longwave and shortwave radiation, and turbulent heat fluxes for the period 1958–2023 from RACMO (5.5 km) and MAR. Besides, there is a slight difference in the GrIS area in the two RCMs, and the areas of the GICs in RACMO and MAR are 8.1×10^4 km^2 and 7.6×10^4 km^2, respectively.

2.2 Performance of modeling surface melt rates

Previous studies have proven good performance of RACMO and MAR in simulating the climatology and changes in surface mass balance and other mass components (Noël et al., 2016; Fettweis et al., 2017; Noël et al., 2019). Here, we assessed the model performance in simulating daily surface melt (Fig. A1), using surface melt fluxes (>0 mm w.e./d) from a surface energy balance (SEB) model (Huai et al., 2020), applied in eight automatic weather stations (AWS) at K- and T-transects of west GrIS. Average bias was 0.7 mm w.e./d and average RMSE was 5.1/5.4 mm w.e./d in RACMO/MAR. RCMs have good performance in modelling the Greenland surface melt, and the correlation was significant between RCMs and the SEB model ($R^2 = 0.9$, $p < 0.05$), giving us confidence to examine the long-term changes in Greenland surface melt.

2.3 Capturing extreme events and atmospheric blocking

The 90th percentile of the daily surface melt amount is chosen as the threshold to define an extreme value, which has been widely used (Leeson et al., 2018; Mattingly et al., 2020; Wang and Luo, 2022). Each date in the calendar year has a separate threshold, based on the distribution of daily surface melt of that calendar date of the 66-year time series, as used in McLeod and Mote (2016). This approach takes into account the annual cycle of surface melt to avoid all extreme events being concentrated in similar calendar periods every year.

There are many blocking indices applied to assess the impact of large-scale atmospheric circulation on Greenland climate changes (Wachowicz et al., 2021). The original Greenland blocking index (GBI, Hanna et al., 2016) represents the average 500 hPa geopotential height over a domain situated over Greenland. Here we used an updated version, GBI_Z (Hanna et al., 2018), again based on the average 500 hPa geopotential height from the latest atmospheric reanalysis ERA5, but removing the zonal average. Then, we utilized the 90th percentile of the distribution of 1958–2023 daily GBI_Z as the threshold to identify blocking events.

2.4 Anomalies in extreme events

The average anomalies for extreme events were computed by subtracting the average for non-extreme events. For the comparison of extreme events between different periods, we first compared the variables to the average conditions of the corresponding period without extreme events and then compared the anomalies between different periods.

3. Results

3.1 Characteristics of Greenland surface melt

Fig. 1a shows the monthly relative fraction from April to October of Greenland surface melt rates. Surface melt predominantly happens in summer (June to August), with a proportion of 85%/92% from RACMO/MAR. However, satellite data have confirmed the earlier onset date of melting (Colosio et al., 2021). Doyle et al. (2015) also reported that increased rainfall could induce the occurrence of surface melt in September. With the air warming, there are more rainfall events over the GrIS, especially in the late summer and September (Huai et al., 2022). In August 2022, rainfall even occurred at the Summit station (Box et al., 2022; Dou et al., 2023). Therefore, with Greenland air temperature rising and rainfall events increasing, surface melt in May and September cannot be neglected even when in the current climate their contribution proportion is relatively low. They will play a more important role and are included in the analysis here.

Fig. 1b and c show the spatial distribution of long-term (1958–2023) average annual total surface melt. The areas of high annual total melt are mainly concentrated in the ablation zone along the margins of the GrIS and GICs. At the western and southern edge of the ice sheet, annual surface melt exceeds 2000 mm w.e. At the lower parts of the Qagssimiut lobe in the southern GrIS (black square box in Fig. 1b and c), annual surface melt even exceeds 4000 mm w.e. The multi-year average Greenland annual surface melt from 1958 to 2023 was 650/531 Gt in RACMO/MAR. MAR underestimated Greenland surface melt relative to RACMO, which was also reported by Zheng et al. (2022). Here, 80% of the difference in total surface melt integrated between the two RCMs results from the difference in the GrIS, especially eastern regions where the topography is very complicated and high-resolution RACMO has more areas with high surface melt, benefit from statistical downscaling, relative to the version of MAR used here.

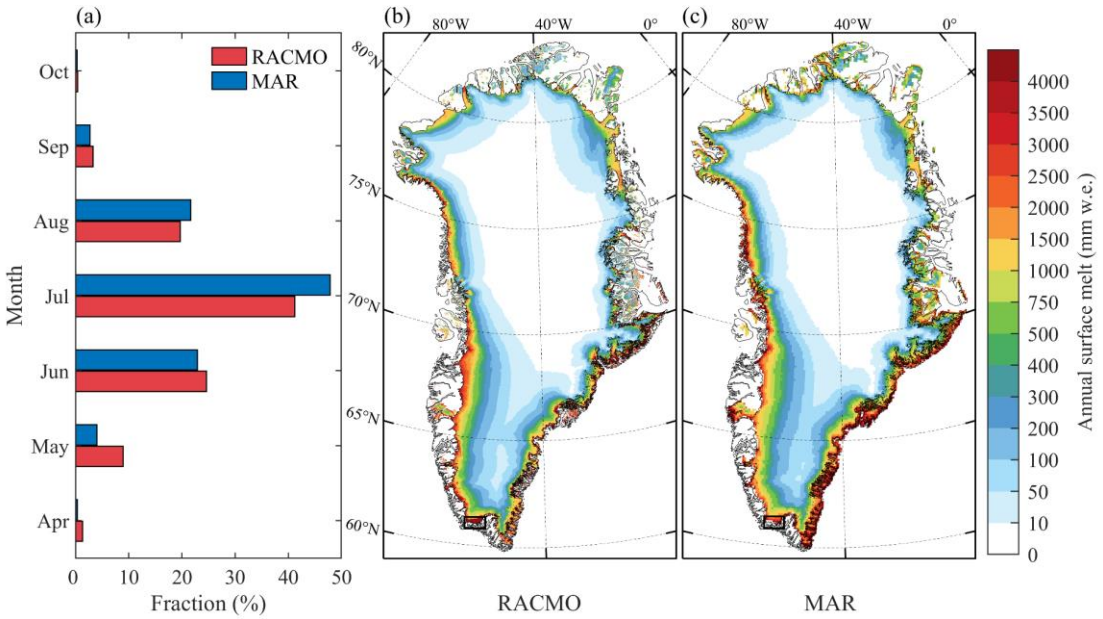

Fig. 1 Characteristics of modeling surface melt in Greenland, (a) monthly fraction (April to October) distribution of surface melt (1958–2023 mean), spatial distribution of multi-year averaged annual total surface melt from (b) RACMO and (c) MAR (Black square boxes represent the Qagssimiut lobe).

3.2 Changes in annual surface melt

Fig. 2a shows the changes in Greenland annual surface melt relative anomalies relative to 1961–1990. Although there is a difference in annual surface melt rates integrated, average anomalies are highly consistent, with a 1958–2023 average value of 77/82 Gt per year (differ by 6%). To better describe the changes in surface melt, we separated the whole GrIS and GICs into eight individual regions (Fig. 2a), like Niwano et al. (2021). Many investigations of Greenland climate have reported rapid climatic and mass change since the early to mid-1990s. Annual surface melt anomalies also follow this pattern (Fig. 2b), with post-1990 melt trends of 8.6 ± 4.9/7.2 ± 4.4 Gt per year in RACMO/MAR, respectively. Integrated over Greenland, persistent positive melt anomalies relative to 1961–1990 (+152/155 Gt per year on average for RACMO/MAR) have become a major feature post-1990.

Due to the milder climate, SW, SE and SO combined contributed 57%/48% surface melt during 1958–2023 (Tab. A1), while representing only 23%/21% of the entire Greenland. However, the relative surface melt increase in these three southern regions is below average. To reduce the influence of the difference in surface melt magnitude in different individual regions, we presented the relative change (%) in surface melt (Fig. 2c–j). RACMO/MAR reveals a rapid increase trend from 1.1% ± 0.8%/0.6% ± 0.5% per year (SO) to 3.9% ± 1.9%/3.4% ± 1.6 % per year (NO) in south to north individual sectors. Although the total melt in northern Greenland is small relative to the other regions, the relative increase is highly significant. This south–north difference is consistent with changes in the near-surface air temperature and runoff (Noël et al., 2019; Hanna et al., 2021; Zhang et al., 2022).

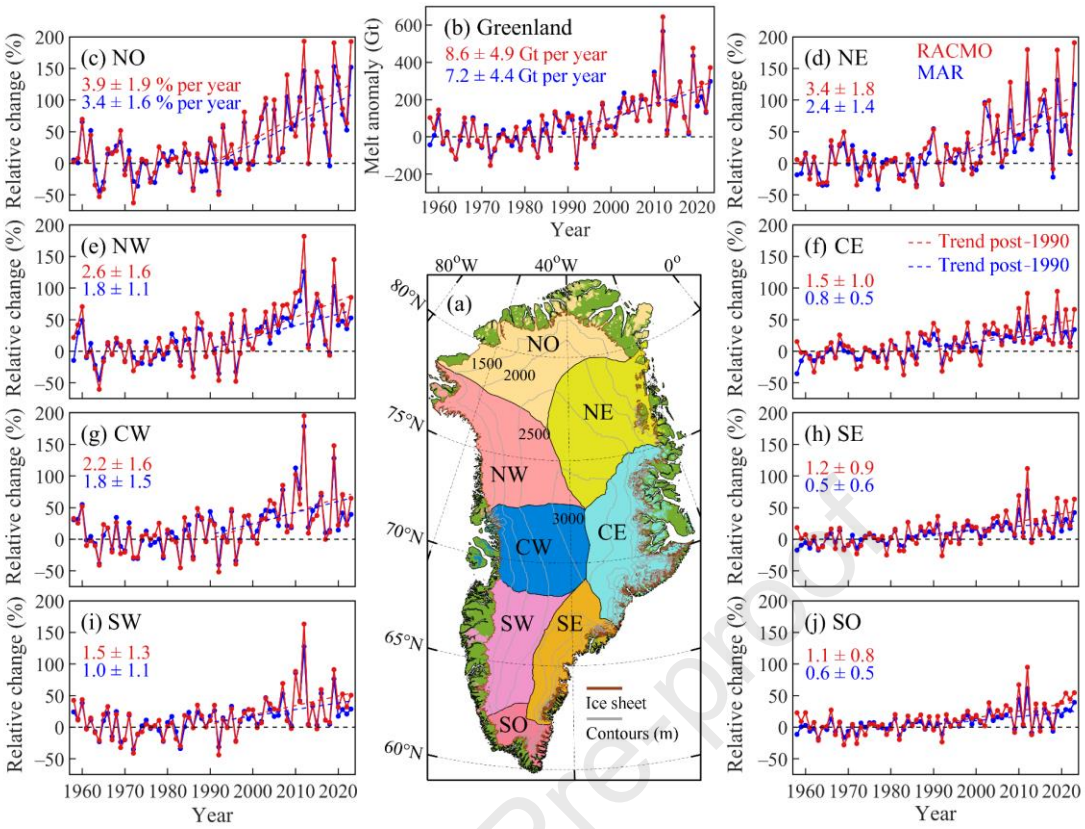

Fig. 2 Changes in annual surface melt and individual sectors, (a) maps of individual sectors, (b) changes in annual surface melt anomalies from RACMO and MAR integrated over the Greenland (GrIS and GICs) during 1958–2023 (relative to 1961–1990), and (c–j) the relative change of annual melt integrated over individual sectors, respectively (relative to 1961–1990; The uncertainty range of linear trends means two standard deviations, *i.e.*, a significance level of 0.05).

The spatial patterns of multi-year melt increase from RACMO and MAR show good agreement (Fig. 3a). The two models differ most in the CE where RACMO has higher annual total melt in CE compared to MAR, possibly due to the steep topography in which the statistical downscaling leads to different results (Noël et al., 2019). To further emphasize the north–south difference, Fig. 3b shows the changes in the contribution of individual sectors to the Greenland total surface melt rates. The contribution of the southern sectors decreased post-1990, while the contribution of the northern sectors increased, especially NO, with its relative melt contributions increasing by 12.9%/19.9% in RACMO/MAR.

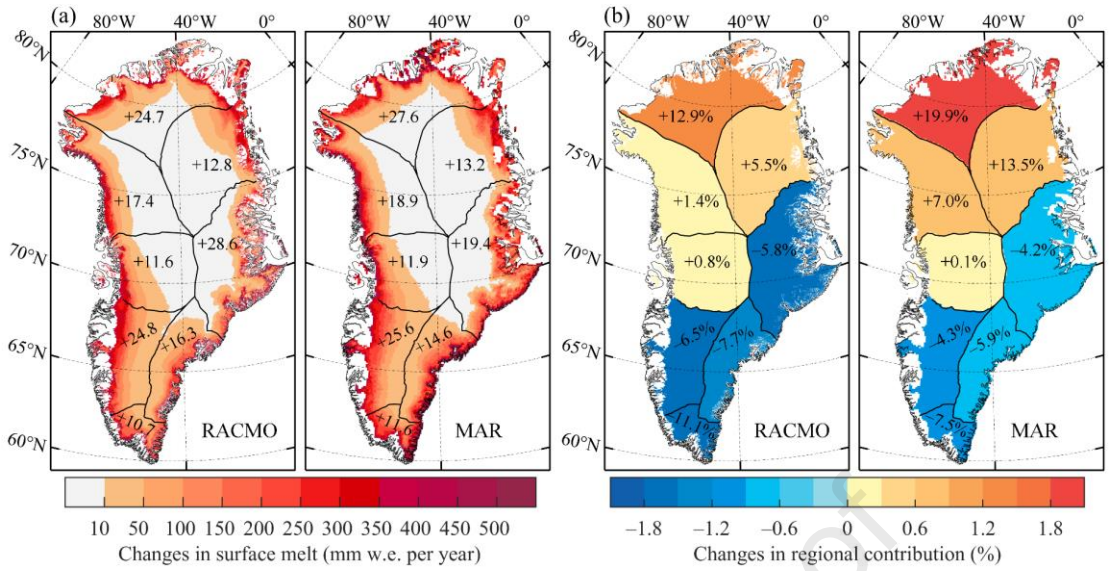

Fig. 3 Interdecadal changes integrated over the individual sectors between 1958–1990 and 1991–2023, (a) averaged annual surface melt from RACMO and MAR, respectively, and (b) regional contribution of individual sectors to the whole Greenland (The numbers listed indicate the relative changes in regional contributions compared to itself).

3.3 Extreme events

Fig. 4 shows that the post-1990 May to September (M–S) probability density distribution of daily surface melt has shifted toward higher amounts (red and blue curves), with the averaged value increasing by 1.0/0.9 Gt/d (+21%/24%). Furthermore, the 90th percentile increased by 2.3/2.2 Gt/d, *i.e.*, approximately 2.3 times the increase in the mean. A more extended right tail suggests more frequent extreme events. Further examination of decadal probability density distributions of daily surface melt indicates that this increase in M–S melt and extreme melt is concentrated in the last two decades (*i.e.*, 2001–2010, 2011–2023) (Fig. A2).

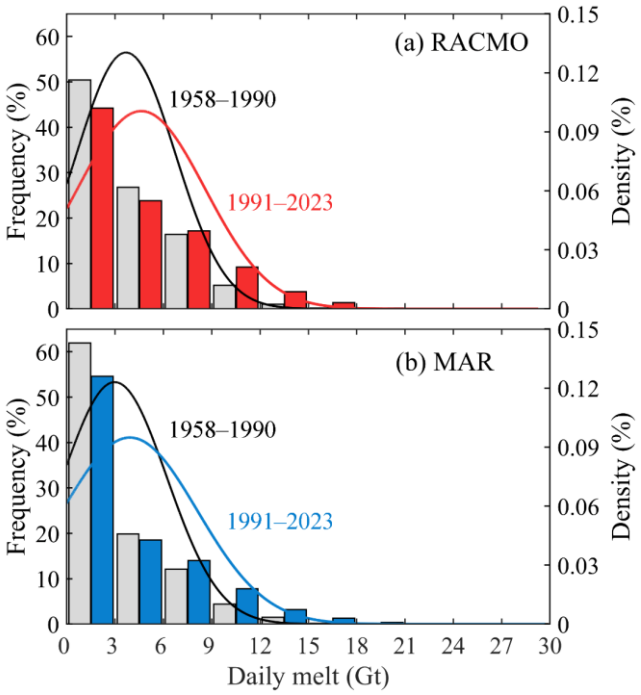

208

209 Fig. 4 Distribution of the integrated daily surface melt in May to September for 1958–1990 and 1991–
210 2023, respectively, from (a) RACMO and (b) MAR.

211 Fig. 5 explores the long-term change of the contribution of extreme events to total melt. Average
212 M–S total extremes rates and frequency during 1958–2023 were 125/114 Gt (Fig. 5a) and 16 d (Fig. 5b),
213 respectively. Extremes contributed 17%/20% of M–S total surface melt (Fig. 5c). Before 1990, no
214 significant trends are observed, but post–1990 totals by extremes and number of days have been
215 increasing by 8.3 ± 5.9/8.3 ± 5.5 Gt per year and 0.7 ± 0.5/0.8 ± 0.5 d per year. With increasing frequency
216 of extreme events and melt amounts, extremes are contributing more to the M–S total surface melt (Fig.
217 5c), with a post–1990 trend of 0.9%/1.1% ± 0.6% per year. Relative to 1958–1990, the fraction of extreme
218 melt has increased by 15%/13%, and now extremes contribute 25%/27% to total surface melt. In the last
219 decade of our study period (2014–2023), the contribution of extreme melt is up to 32% per year. In the
220 extreme melt years of 2012 and 2019 (Nghiem et al., 2012; Tedesco and Fettweis, 2020), extreme events
221 even contribute 78%/82% and 60%/55% of M–S total melt, respectively. Fig. 5d shows that 1991–2023
222 M–S total surface melt in RACMO/MAR has increased by 145/132 Gt per year relative to 1958–1990,
223 while M–S cumulative extreme surface melt has increased by 134/105 Gt per year, *i.e.*, contributing
224 92%/80% to the total change. This means that increasing M–S extremes dominate the increase in the
225 total surface melt.

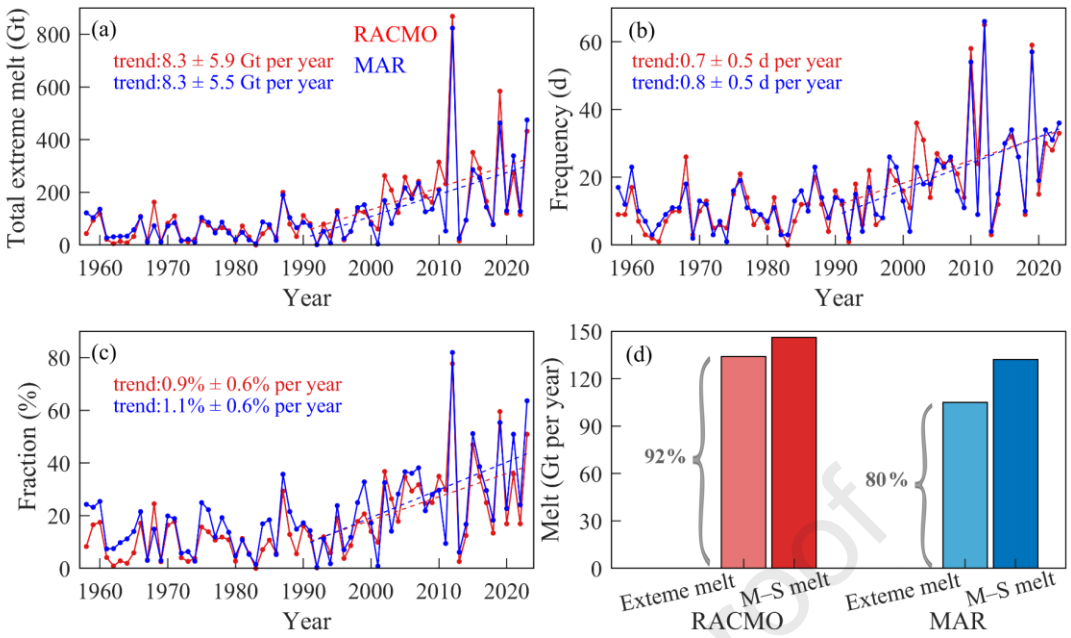

Fig. 5 Changes in Greenland extreme surface melt from May to September during 1958–2023, (a) total extreme surface melt from RACMO and MAR, (b) frequency and (c) the fraction of extreme melt to total M–S melt, and (d) difference in surface melt and extreme melt between 1958–1990 and 1991–2023 (The uncertainty range of linear trends means two standard deviations *i.e.*, a significance level of 0.05).

3.4 Relationship between surface melt and atmospheric circulation

The changes in Greenland climatology and surface mass balance were related with the large-scale circulation, especially the Greenland Blocking (Fettweis et al., 2013; Hanna et al., 2024). Anomalies in M–S surface melt and GBI_Z showed significant correlation (Fig. A3, $r = 0.6$, $p < 0.01$). Here we further showed surface melt and circulation anomalies over Greenland during extreme events. Fig. 6a shows the average surface melt anomalies during M–S extremes relative to non-extreme events. During extreme events, the average daily surface melt in RACMO/MAR was 7.7/7.0 Gt/d, approximately 2.1/2.6 times the value for non-extreme events, concentrated at the edge of the ice sheet. Positive surface melt anomalies are principally related to atmospheric circulation (Fig. 6b), which shows a clear anticyclonic pattern, with southerly winds advecting warm air to the GrIS along its western margin. During extreme events, the atmospheric blocking index (GBI_Z) shows positive ($+1.2\sigma$). This change in circulation increases cloud cover in the northwest, where the ice sheet topography acts as a barrier, but decreases cloud cover in eastern Greenland, where the air descends. Cloud cover anomalies lead to positive anomalies in downward longwave radiation (Fig. 6c). Another important energy source is the increase in net shortwave radiation (Fig. 6d), which mainly results from a decreasing surface albedo (Fig. A4). Surface melt is further enhanced by positive feedbacks such as the snowmelt-albedo feedback as well as the spatial extension of dark, bare-ice regions (Box et al., 2012; Tedesco et al., 2016; Ryan et al., 2019). The advection of warmer air also increases the turbulent sensible heat flux (Fig. 7a). Fig. 7b shows that

the largest anomalous energy input in regions below 2000 m elevation during extreme events was downward longwave radiation, followed by sensible heat flux. Recent studies also reported more atmospheric river events, which increase turbulent fluxes over the melting ice surface, especially in the northeastern GrIS (Mattingly et al., 2018, 2020, 2023). When net energy sources are considered, net shortwave radiation dominates, due to the reduction of upward shortwave radiation.

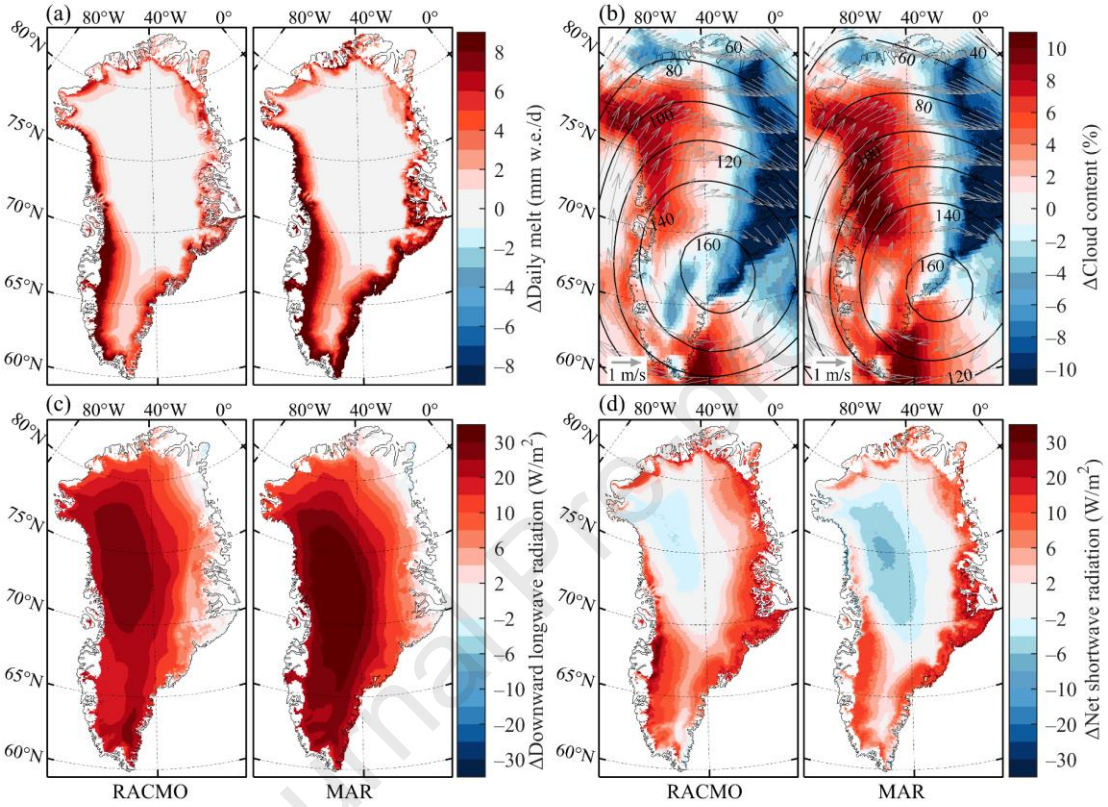

Fig. 6 Average (1958–2023) anomalies during extremes relative to non-extreme melt events, (a) daily surface melt anomaly from RACMO and MAR, (b) 500 hPa geopotential height (contours), wind fields and cloud cover anomalies from ERA5 for extreme events identified by RACMO and MAR, respectively, and (c, d) surface downward longwave radiation and net shortwave radiation anomalies.

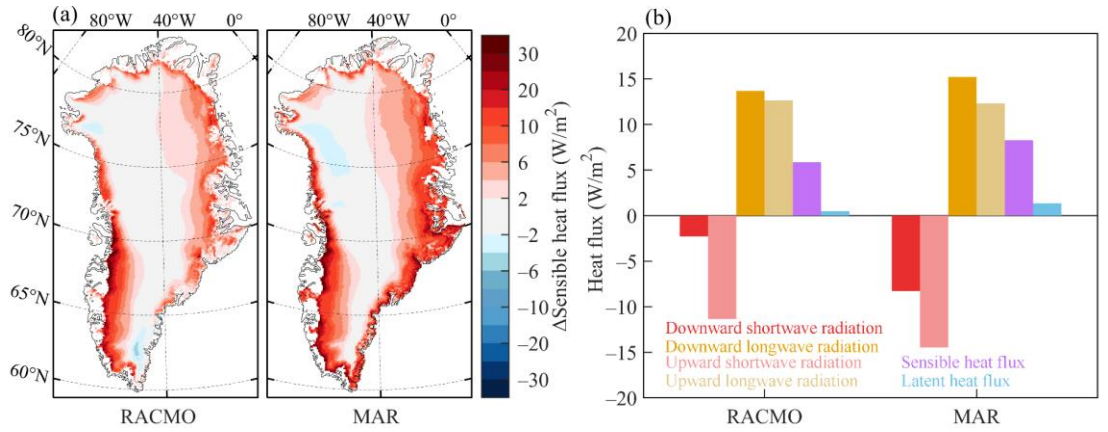

Fig. 7 Average (1958–2023) sensible heat flux anomalies during extremes relative to non-extreme events (a), and specific energy flux statistics energy flux anomalies for regions with elevation below 2000 m (b).

Increasing extreme surface melt events on the one hand were related with more frequent atmospheric blocking in M–S post-1990 ($r = 0.8/0.7, p < 0.01$) (Fig. 8). Frequent blocking caused energy fluxes anomalies shown in Fig. 6 and Fig. 7 and then intensified surface melt in Greenland. In fact, the increase in extreme melt rates, on the other hand, results from the enhanced intensity of extremes. Fig. 9 shows how the nature of extreme events changed post-1990. Average extreme melt rates post–1990 increase by 11%/12% in RACMO/MAR, mainly in northern Greenland, compared with 1958–1990 (Fig. 9a). This north–south division is also reflected in the changes in 500 hPa geopotential height and cloud cover (Fig. 9b). Compared with 1958–1990, anticyclonic conditions centred in the southeast have weakened and the summer average 500 hPa geopotential has increased more in western areas (Noël et al., 2019). The increase in cloud cover in the northern Greenland enhanced downward longwave radiation (Fig. 9c), while descending air and the consequent adiabatic heating increased sensible heat flux (Fig. 9d). In the southern Greenland, the reduced cloud cover decreases downward longwave radiation and the advection of colder air from the north reduces sensible heat flux which mostly offset the downward shortwave radiation increase (Fig. A5) so that the strength of extreme events hardly changed there.

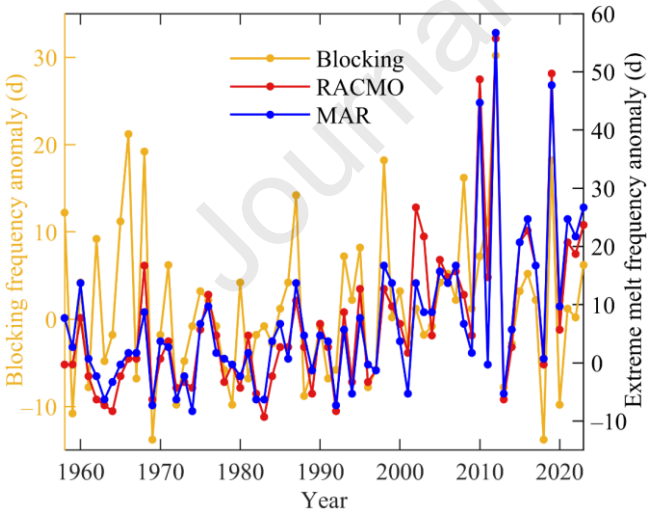

Fig. 8 Changes in the occurrence frequency anomalies relative to the average of 1961–1990 of blocking and melt extremes in May to September.

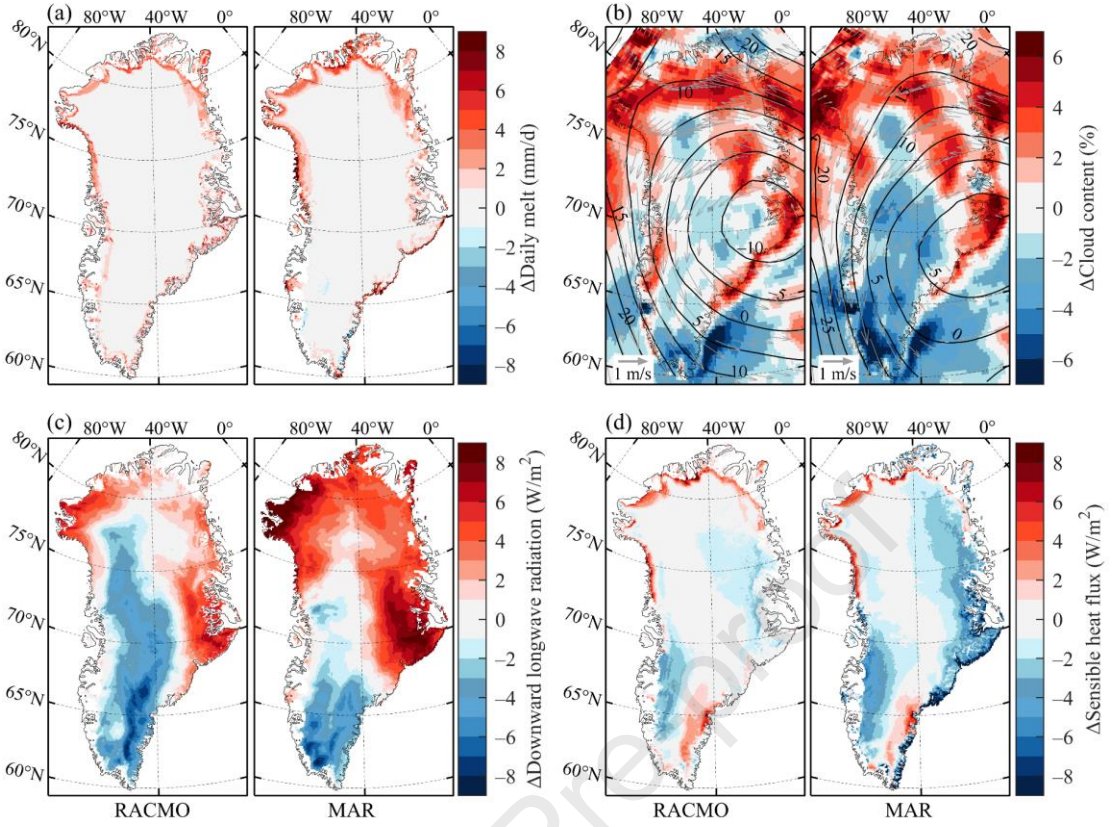

Fig. 9 Difference in extreme melt events before and after 1990 (1991–2023 minus 1958–1990), (a) daily surface melt during extreme melt events, (b) 500 hPa geopotential height, wind fields and cloud cover, (c) downward longwave radiation, and (d) surface sensible heat flux.

4. Discussion

Because satellite data cannot directly observe surface melt rate, Greenland surface melt rate has not been understood in the past. Based on two high-resolution regional climate models, here we showed the variations in surface melt rate during 1958–2023. We found that Greenland surface melt rates have been increasing post-1990, which is related with higher relative increase in northern regions and more frequent extreme events. The dominant role of extreme events in the total increase in M–S surface melt. These extreme events here were attributed to increasing downward longwave radiation, sensible heat flux and the reduction of upward shortwave radiation. Many studies stressed the dominant contribution of net shortwave radiation rather than longwave radiation in the increase in the summer surface melt and extremes (Hofer et al., 2017; Bonsoms et al., 2024). Our results support this but also show that extremes have remarkably higher downward longwave radiation and sensible heat flux. Increasing downward longwave radiation and sensible heat flux have amplified surface melt in Greenland and made surface melt events more extreme. Wang et al. (2021) found that for >3σ melt events the day-to-day variability of surface melt is dominated by sensible heat flux. Particularly, Ward et al. (2020) found that sensible heat flux was more critical for increasing surface melt when the centre of blocking was situated in the southeast. Fig. 10 further shows the surface energy balance anomalies in each region during M–S melt

extremes relative to non-extreme events during 1958–2023. For the surface energy inputs, the increasing downward longwave radiation was the largest contributor, followed by sensible heat flux in most regions. In the NW regions, longwave radiation even dominated the increase in extreme surface melt rates rather than net shortwave radiation. Our results showed that with the Greenland warming, the decline in albedo had made surface melt naturally higher, while the increase in longwave radiation and sensible heat fluxes resulting from circulation anomalies had amplified surface melt events and made them extreme. It will improve our understanding of extreme surface melt events and the mechanisms.

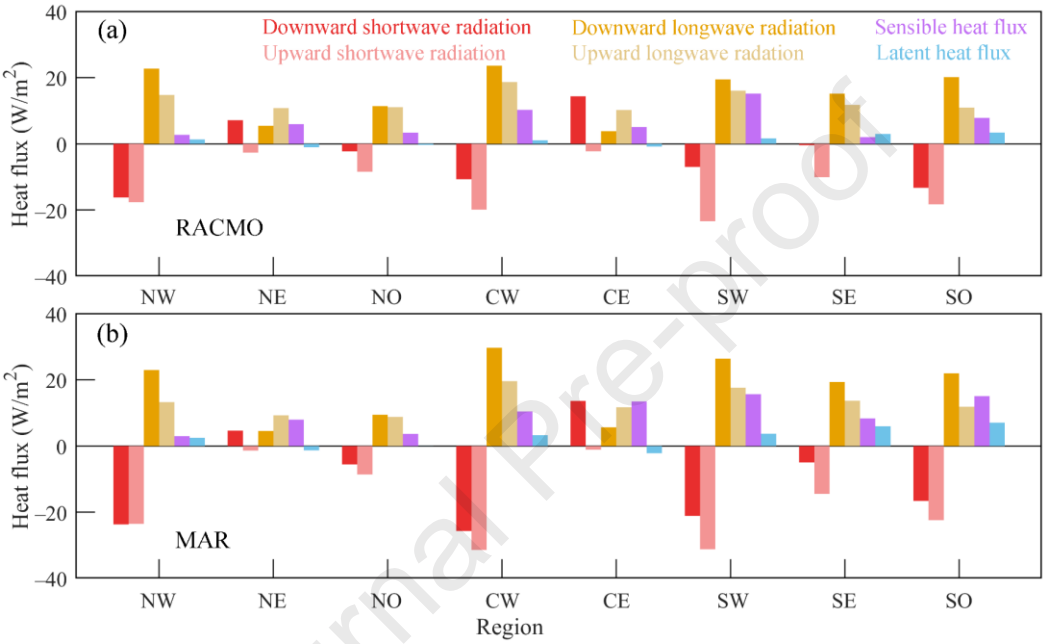

Fig. 10 Average (1958–2023) energy heat flux anomalies during extreme events in each region below 2000 m a.s.l.

Our results contribute to enhancing the comprehension of long-term variations in Greenland surface melt, particularly regarding spatial patterns and extreme events. However, our results also show some limitations and uncertainties. For the annual surface melt rate, we noted that RACMO/MAR 1958–2023 annual mean integrated surface melt differs by 22%. The difference is related to spatial resolution in models. The main source of difference originates from the CE region, where downscaled RACMO has higher surface melt outputs (+59 Gt per year, Table. A1). Eighty-three percent of the difference in CE comes from the bias over the GrIS, with more surface melt rates in RACMO relative to MAR (Table. A2). Fig. 11 shows the CE elevation-area and elevation melt distribution. The total area in the two RCMs is consistent while RACMO has more areas below 300 m and below 1300 m melt in RACMO is approximately twice that in MAR. Statistical downscaling in RACMO (version of 1 km) greatly increases surface melt in the CE sector (Noël et al., 2016). The difference between regional climate models has limited further discussion about spatial variations, especially in the margins, and then results in some uncertainties in surface melt. Because of this difference in integrated surface melt rates, we cannot more

accurately estimate the refreezing and consequent runoff over the GrIS. This indicates the importance of improving the performance of modelling surface melt in complex-topography areas and consistency between climate models.

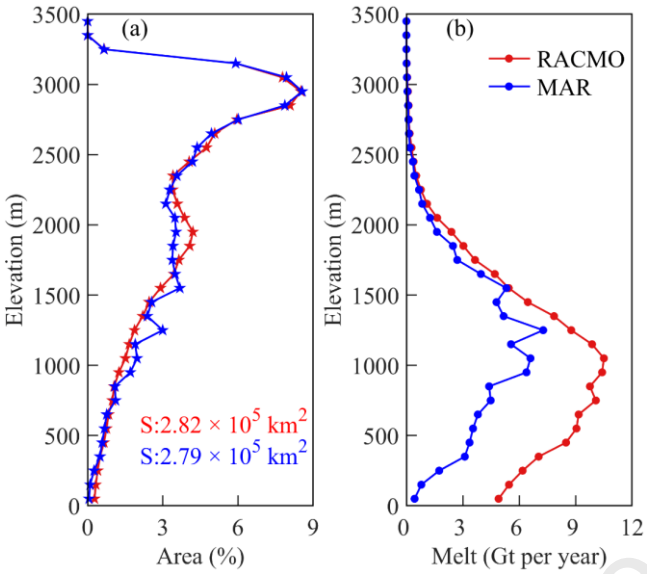

Fig. 11 The distribution of (a) area (%) and (b) cumulative surface melt for different CE elevation zones during 1958–2023 (The numbers in (a) represent the total area of CE regions).

These results suggest that if we want to more accurately project future sea level rise from Greenland surface melting, more research into extreme events in relation to atmospheric circulation anomalies is needed. Additionally, we need to further improve the simulation of extreme events in Greenland and the performance of models in topographically rough regions like southeastern Greenland.

5. Conclusions

We used two high-resolution regional climate models (RACMO2.3p2 and MARv3.14) to analyze the variations in Greenland surface melt from 1958 to 2023. RACMO and MAR show good consistency in long-term variations in Greenland surface melt rates. We found that annual surface melt has significantly increased post-1990 at a rate of 8.6 ± 4.9/7.2 ± 4.4 Gt per year by RACMO/MAR. Compared with southern regions, the northern regions showed a stronger regional relative increase rate post-1990 (3.9% ± 1.9%/3.4% ± 1.6% per year) and was contributing more surface melt to the whole Greenland.

The increase in total surface melt is relevant to frequent extreme surface melt events. Extreme melt events from May to September (M–S) have become more frequent post-1990 (0.7/0.8 ± 0.5 d per year), with stronger intensity (+11%/12%). M–S melt from extreme events has increased by 134/105 Gt per year post-1990 and dominates the increase in the total surface melt. The increase in downward longwave radiation, net shortwave radiation and sensible heat flux caused the occurrence of extreme events.

Meanwhile, the recent rise in surface melt and extreme events is linked to more frequent atmospheric blocking in recent decades.

Declaration of competing interest

The authors declare no conflict of interest.

CRediT authorship contribution statement

Qing-Lin Zhang: Software, Visualization, Formal analysis, Writing-Original Draft. **Ming-Hu Ding**: Conceptualization, Writing-Review & Editing, Supervision, Project administration. **Michiel R. van den Broeke**: Resources, Data Curation, Writing-Review & Editing. **Brice Noël**: Resources, Data Curation, Writing-Review & Editing. **Xavier Fettweis**: Resources, Data Curation, Writing-Review & Editing. **Sai Wang**: Conceptualization, Writing-Review & Editing. **Wei-Jun Sun**: Writing-Review & Editing. **Qing-Long You**: Writing-Review & Editing. **Cun-De Xiao**: Writing-Review & Editing. **Da-He Qin**: Writing-Review & Editing. **Bao-Juan Huai**: Conceptualization, Writing-Review & Editing, Supervision.

Acknowledgments

The study was supported financially by the National Science Foundation of China (42171121), the Outstanding Youth Fund project of Shandong province (ZR2023YQ035), and the Basic Research Fund of the Chinese Academy Meteorological and Sciences (2023Z025, 2023Z004 & 2023Z015). M. R. van den Broeke acknowledges the support of the Netherlands Earth System Science Centre (NESSC). B. Noël is a Research Associate of the Fonds de la Recherche Scientifique de Belgique–F.R.S.-FNRS.

References

Antwerpen, R.M., Tedesco, M., Fettweis, X., et al., 2022. Assessing bare-ice albedo simulated by MAR over the Greenland ice sheet (2000–2021) and implications for meltwater production estimates. Cryosphere 16(10), 4185–4199.

Beckmann, J., Winkelmann, R., 2023. Effects of extreme melt events on ice flow and sea level rise of the Greenland Ice Sheet. Cryosphere 17(7), 3083–3099.

Bonsoms, J., Oliva, M., López-Moreno, J.I., et al., 2024. Rising extreme meltwater trends in Greenland ice sheet (1950–2022): surface energy balance and large-scale circulation changes. J. Clim. 37(18), 4851–4866.

Box, J.E., Fettweis, X., Stroeve, J.C., et al., 2012. Greenland ice sheet albedo feedback: thermodynamics and atmospheric drivers. Cryosphere 6, 821–839.

Box, J.E., Wehrlé, A., van As, D., et al., 2022. Greenland ice sheet rainfall, heat and albedo feedback impacts from the mid-August 2021 atmospheric river. Geophys. Res. Lett. 49(11), e2021GL097356.

Chen, X., Zhang, X., Church, J.A., et al., 2017. The increasing rate of global mean sea-level rise during 1993–2014. Nat. Clim. Change 7(7), 492–495.

Choi, Y., Morlighem, M., Rignot, E., et al., 2021. Ice dynamics will remain a primary driver of Greenland ice sheet mass loss over the next century. Commun. Earth Environ. 2(1), 26.

Colosio, P., Tedesco, M., Fettweis, X., et al., 2021. Surface melting over the Greenland ice sheet from enhanced resolution passive microwave brightness temperatures (1979–2019). Cryosphere 15, 2623–2646.

de Ridder, K., Gallée, H., 1998. Land surface-induced regional climate change in southern Israel. J. Appl. Meteorol. Climatol. 37(11), 1470–1485.

Dobricic, S., Russo, S., Pozzoli, L., et al., 2020. Increasing occurrence of heat waves in the terrestrial Arctic. Environ. Res. Lett. 15(2), 024022.

Dou, T., Xie, Z., Box, J.E., et al., 2023. Analysis of the record-breaking August 2021 rainfall over the Greenland Ice Sheet. Adv. Polar Sci. 34(3), 165–176.

Doyle, S.H., Hubbard, A., van de Wal, R.S., et al., 2015. Amplified melt and flow of the Greenland ice sheet driven by late-summer cyclonic rainfall. Nat. Geosci. 8(8), 647–653.

Ettema, J., van den Broeke, M., van Meijgaard, E., et al., 2010. Climate of the Greenland ice sheet using a high-resolution climate model. Part 1: evaluation. Cryosphere 4(4), 511–527.

Fettweis, X., Hanna, E., Lang, C., et al., 2013. Brief communication "Important role of the mid-tropospheric atmospheric circulation in the recent surface melt increase over the Greenland ice sheet". Cryosphere 7(1), 241–248.

Fettweis, X., Box, J.E., Agosta, C., et al., 2017. Reconstructions of the 1900–2015 Greenland ice sheet surface mass balance using the regional climate MAR model. Cryosphere 11(2), 1015–1033.

Fettweis, X., Hofer, S., Krebs-Kanzow, U., et al., 2020. GrSMBMIP: intercomparison of the modelled 1980–2012 surface mass balance over the Greenland Ice Sheet. Cryosphere 14(11), 3935–3958.

Frederikse, T., Landerer, F., Caron, L., et al., 2020. The causes of sea-level rise since 1900. Nature 584(7821), 393–397.

Gallée, H., Duynkerke, P.G., 1997. Air–snow interactions and the surface energy and mass balance over the melting zone of west Greenland during the Greenland Ice Margin Experiment. J. Geophys. Res. Atmos. 102(D12), 13813–13824.

Gallée, H., Guyomarc'h, G., Brun, E., 2001. Impact of snow drift on the Antarctic ice sheet surface mass balance: possible sensitivity to snow-surface properties. Bound. Layer Meteor. 99, 1–19.

Greuell, W., Konzelmann, T., 1994. Numerical modelling of the energy balance and the englacial temperature of the Greenland Ice Sheet: calculations for the ETH-Camp location (West Greenland, 1155 m asl). Global Planet. Change 9(1–2), 91–114.

Hanna, E., Cropper, T.E., Hall, R.J., et al., 2016. Greenland Blocking Index 1851–2015: a regional climate change signal. Int. J. Climatol. 36(15), 4847–4861.

Hanna, E., Fettweis, X., Hall, R.J., 2018. Brief communication: recent changes in summer Greenland blocking captured by none of the CMIP5 models. Cryosphere 12(10), 3287–3292.

Hanna, E., Cappelen, J., Fettweis, X., et al., 2021. Greenland surface air temperature changes from 1981 to 2019 and implications for ice-sheet melt and mass-balance change. Int. J. Climatol. 41, E1336–E1352.

Hanna, E., Topál, D., Box, J.E., et al., 2024. Short- and long-term variability of the Antarctic and Greenland ice sheets. Nat. Rev. Earth Environ. 5(3), 193–210.

Hofer, S., Tedstone, A.J., Fettweis, X., et al., 2017. Decreasing cloud cover drives the recent mass loss on the Greenland Ice Sheet. Sci. Adv. 3(6), e1700584.

Huai, B., van den Broeke, M.R., Reijmer, C.H., 2020. Long-term surface energy balance of the western Greenland Ice Sheet and the role of large-scale circulation variability. Cryosphere 14(11), 4181–4199.

Huai, B., van den Broeke, M.R., Reijmer, C.H., et al., 2022. A daily 1-km resolution Greenland rainfall climatology (1958–2020) from statistical downscaling of a regional atmospheric climate model. J. Geophys. Res. Atmos. 127(17), e2022JD036688.

IMBIE (Ice sheet Mass Balance Inter-comparison Exercise) Team, 2020. Mass balance of the Greenland Ice Sheet from 1992 to 2018. Nature 579(7798), 233–239.

Leeson, A.A., Eastoe, E., Fettweis, X., 2018. Extreme temperature events on Greenland in observations and the MAR regional climate model. Cryosphere 12(3), 1091–1102.

Lefebre, F., Gallée, H., van Ypersele, J.P., et al., 2003. Modeling of snow and ice melt at ETH Camp (West Greenland): a study of surface albedo. J. Geophys. Res. Atmos. 108(D8). https://doi.org/10.1029/2001JD001160.

Ligtenberg, S.R., Kuipers Munneke, P., Noël, B.P., et al., 2018. Brief communication: improved simulation of the present-day Greenland firn layer (1960–2016). Cryosphere 12(5), 1643–1649.

Mattingly, K.S., Mote, T.L., Fettweis, X., 2018. Atmospheric river impacts on Greenland Ice Sheet surface mass balance. J. Geophys. Res. Atmos. 123, 8538–8560.

Mattingly, K.S., Mote, T.L., Fettweis, X., et al., 2020. Strong summer atmospheric rivers trigger Greenland Ice Sheet melt through spatially varying surface energy balance and cloud regimes. J. Clim. 33(16), 6809–6832.

Mattingly, K.S., Turton, J.V., Wille, J.D., et al., 2023. Increasing extreme melt in northeast Greenland linked to foehn winds and atmospheric rivers. Nat. Commun. 14, 1743.

McLeod, J.T., Mote, T.L., 2016. Linking interannual variability in extreme Greenland blocking episodes to the recent increase in summer melting across the Greenland ice sheet. Int. J. Climatol. 36(3). doi:10.1002/joc.4440.

Meredith, M.P., Sommerkorn, M., Cassotta, S., et al., 2019. Polar regions. In: IPCC (Ed.), The Ocean and Cryosphere in a Changing Climate: Summary for Policymakers. Cambridge University Press, Cambridge, and New York. https://doi.org/10.1017/9781009157964.005.

Mernild, S.H., Mote, T.L., Liston, G.E., 2011. Greenland ice sheet surface melt extent and trends: 1960–2010. J. Glaciol. 57(204), 621–628.

Nghiem, S., Hall, D., Mote, T., et al., 2012. The extreme melt across the Greenland ice sheet in 2012. Geophys. Res. Lett., 39, L20502.

Niwano, M., Box, J.E., Wehrlé, A., et al., 2021. Rainfall on the Greenland ice sheet: present-day climatology from a high-resolution non-hydrostatic polar regional climate model. Geophys. Res. Lett. 48, e2021GL092942.

Noël, B., van de Berg, W., van Meijgaard, E., et al., 2015. Evaluation of the updated regional climate model RACMO2.3: summer snowfall impact on the Greenland Ice Sheet. Cryosphere 9(5), 1831–1844.

Noël, B., van de Berg, W.J., Machguth, H., et al., 2016. A daily, 1 km resolution data set of downscaled Greenland ice sheet surface mass balance (1958–2015). Cryosphere 10(5), 2361–2377.

Noël, B., van de Berg, W.J., Lhermitte, S., et al., 2017. A tipping point in refreezing accelerates mass loss of Greenland's glaciers and ice caps. Nat. Commun. 8(1), 1–8.

Noël, B., van de Berg, W.J., van Wessem, J.M., et al., 2018. Modelling the climate and surface mass balance of polar ice sheets using RACMO2. Part 1: Greenland (1958–2016). Cryosphere 12(3), 811–831.

Noël, B., van de Berg, W.J., Lhermitte, S., et al., 2019. Rapid ablation zone expansion amplifies north Greenland mass loss. Sci. Adv. 5(9), eaaw0123.

Otosaka, I.N., Shepherd, A., Ivins, E.R., et al., 2023. Mass balance of the Greenland and Antarctic ice sheets from 1992 to 2020. Earth Syst. Sci. Data 15, 1597–1616.

Overland, J.E., Wang, M., 2021. The 2020 Siberian heat wave. Int. J. Climatol. 41(S1), E2341–E2346.

Previdi, M., Smith, K.L., Polvani, L.M., 2021. Arctic amplification of climate change: a review of underlying mechanisms. Environ. Res. Lett. 16(9), 093003.

Ryan, J.C., Smith, L.C., van As, D., et al., 2019. Greenland Ice Sheet surface melt amplified by snowline migration and bare ice exposure. Sci. Adv. 5, eaav3738.

Serreze, M.C., Barry, R.G., 2011. Processes and impacts of Arctic amplification: a research synthesis. Global Planet. Change 77(1–2), 85–96.

Tedesco, M., Doherty, S., Fettweis, X., et al., 2016. The darkening of the Greenland Ice Sheet: trends, drivers, and projections (1981–2100). Cryosphere 10, 477–496.

Tedesco, M., Fettweis, X., 2020. Unprecedented atmospheric conditions (1948–2019) drive the 2019 exceptional melting season over the Greenland ice sheet. Cryosphere 14(4), 1209–1223.

van den Broeke, M.R., Enderlin, E.M., Howat, I.M., et al., 2016. On the recent contribution of the Greenland ice sheet to sea level change. Cryosphere 10(5), 1933–1946.

van den Broeke, M.R., Kuipers Munneke, P., Noël, B., et al., 2023. Contrasting current and future surface melt rates on the ice sheets of Greenland and Antarctica: lessons from in situ observations and climate models. PLOS Clim. 2(5), e0000203.

van Wessem, J.M., van de Berg, W.J., Noël, B.P., et al., 2018. Modelling the climate and surface mass balance of polar ice sheets using RACMO2. Part 2: Antarctica (1979–2016). Cryosphere 12(4), 1479–1498.

Wachowicz, L.J., Preece, J.R., Mote, T.L., et al., 2021. Historical trends of seasonal Greenland blocking under different blocking metrics. Int. J. Climatol. 41, E3263–E3278.

Walsh, J.E., Ballinger, T.J., Euskirchen, E.S., et al., 2020. Extreme weather and climate events in northern areas: a review. Earth Sci. Rev. 209, 103324.

Wang, H., Luo, D., 2022. North Atlantic footprint of summer Greenland ice sheet melting on interannual to interdecadal time scales: a Greenland blocking perspective. J. Clim. 35(6), 1939–1961.

Wang, W., Zender, C.S., van As, D., et al., 2021. Greenland surface melt dominated by solar and sensible heating. Geophys. Res. Lett. 48(7), e2020GL090653. https://doi.org/10.1029/2020GL090653

Ward, J.L., Flanner, M.G., Dunn-Sigouin, E., 2020. Impacts of Greenland block location on clouds and surface energy fluxes over the Greenland Ice Sheet. J. Geophys. Res. Atmos. 125(22), e2020JD033172. https://doi.org/10.1029/2020JD033172

Zhang, Q., Huai, B., van den Broeke, M.R., et al., 2022. Temporal and spatial variability in contemporary Greenland warming (1958–2020). J. Clim. 35(9), 2755–2767.

Zheng, L., Cheng, X., Shang, X., et al., 2022. Greenland ice sheet daily surface melt flux observed from space. Geophys. Res. Lett. 49(6), e2021GL096690.

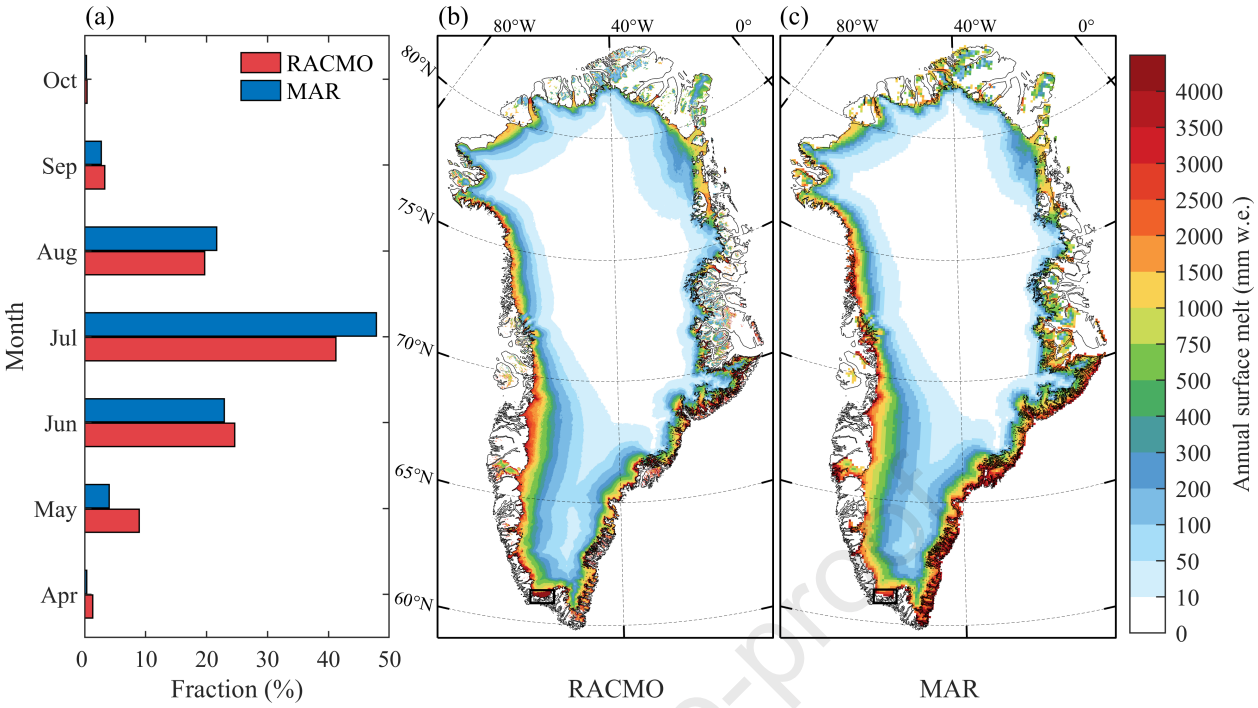

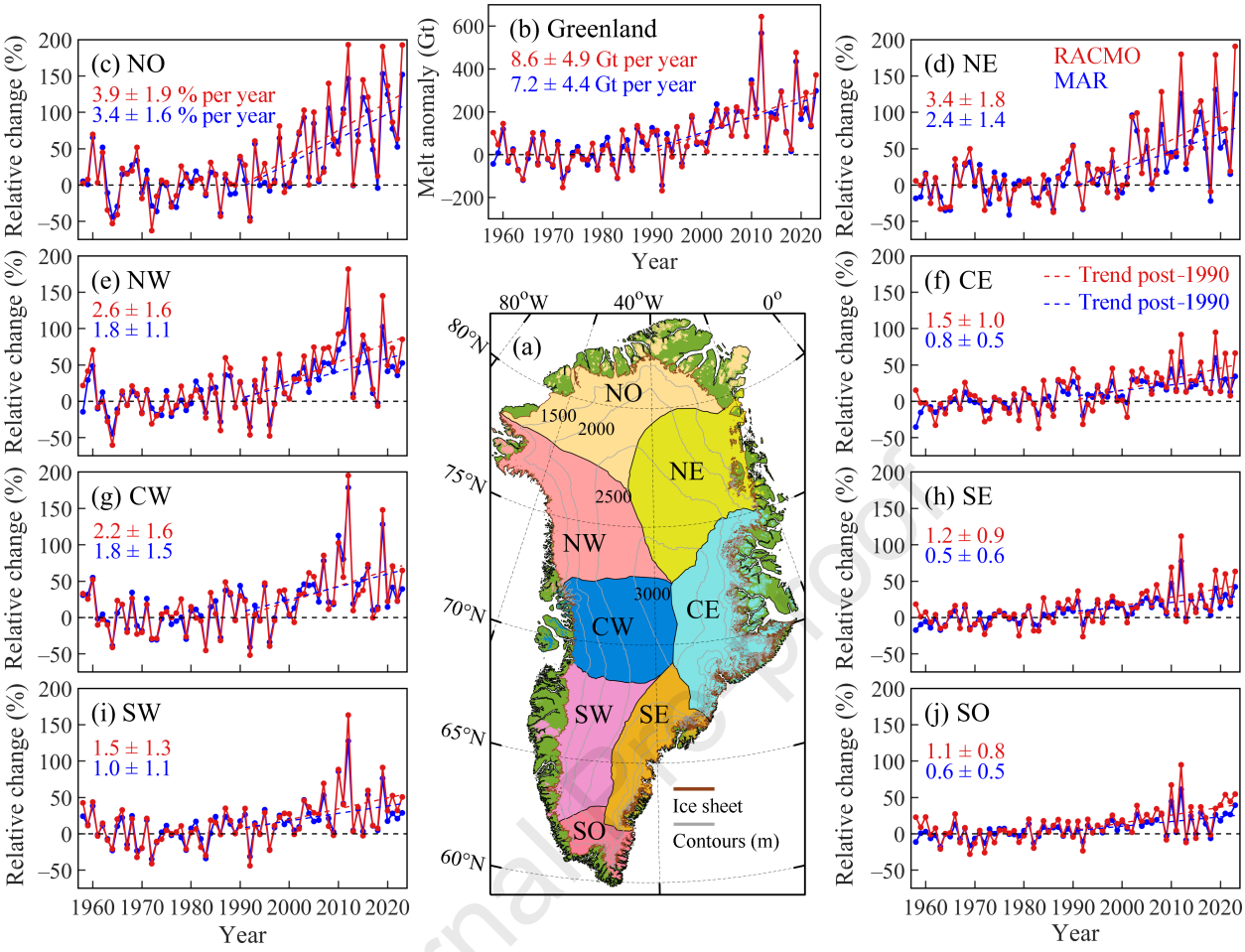

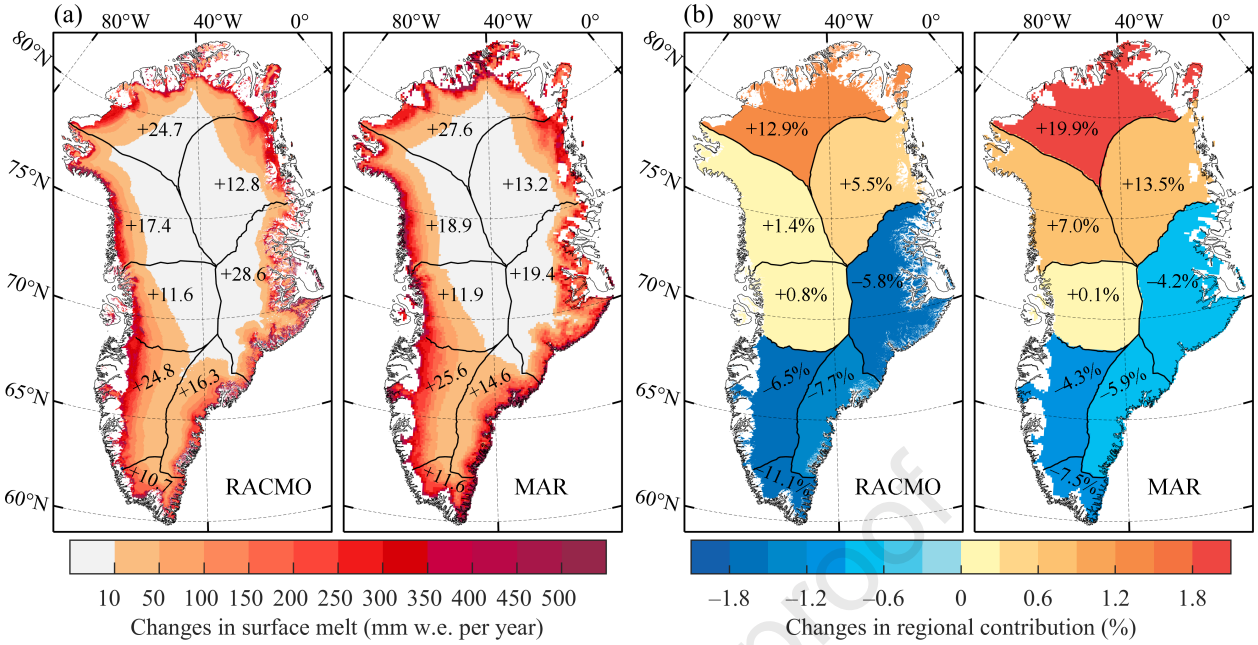

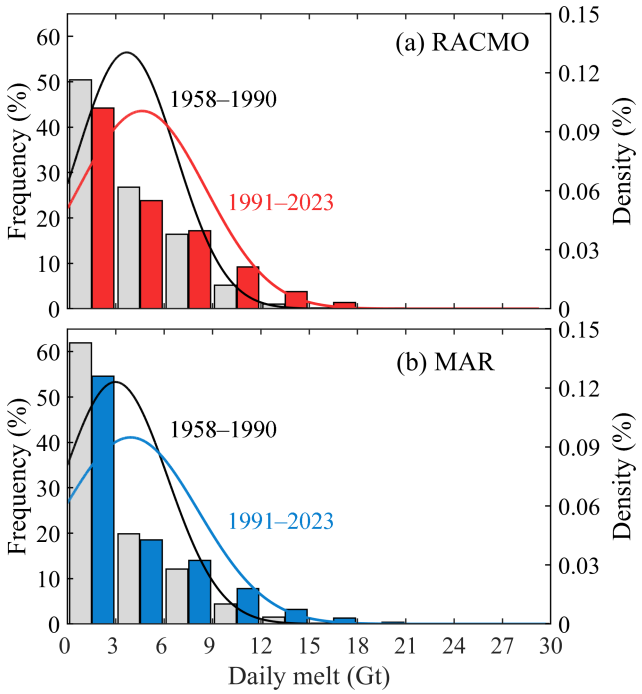

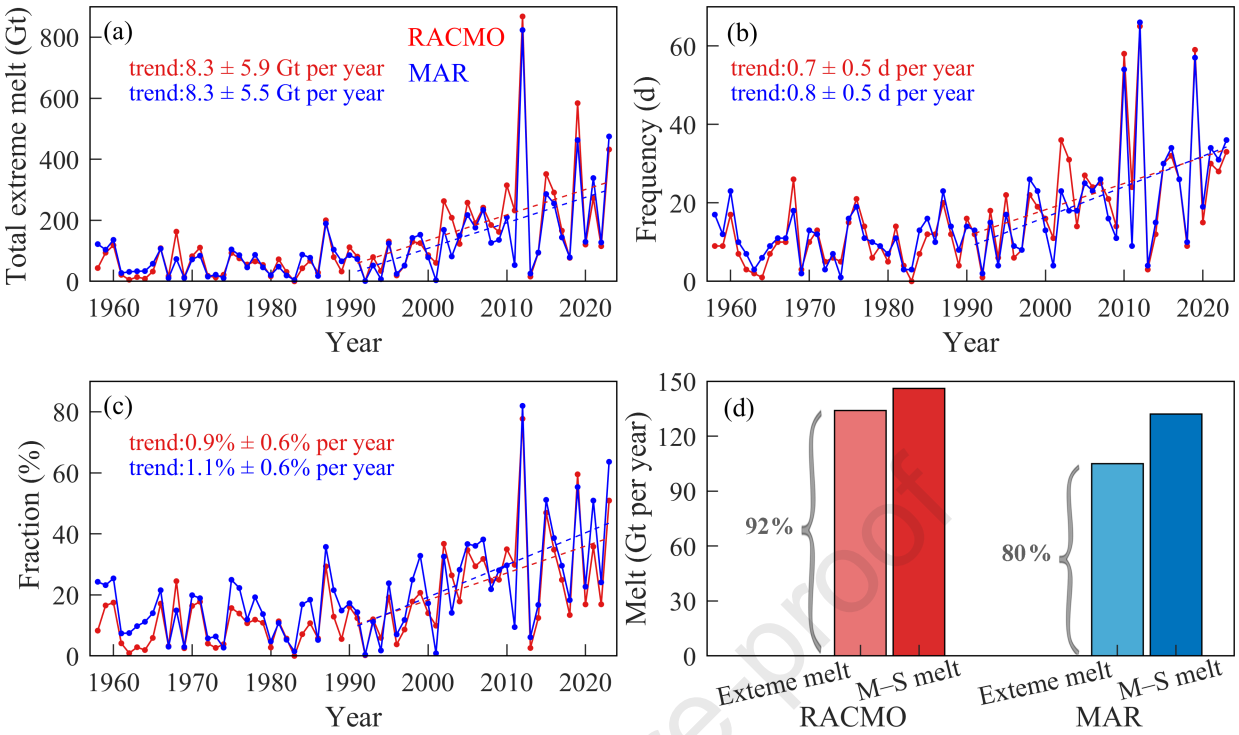

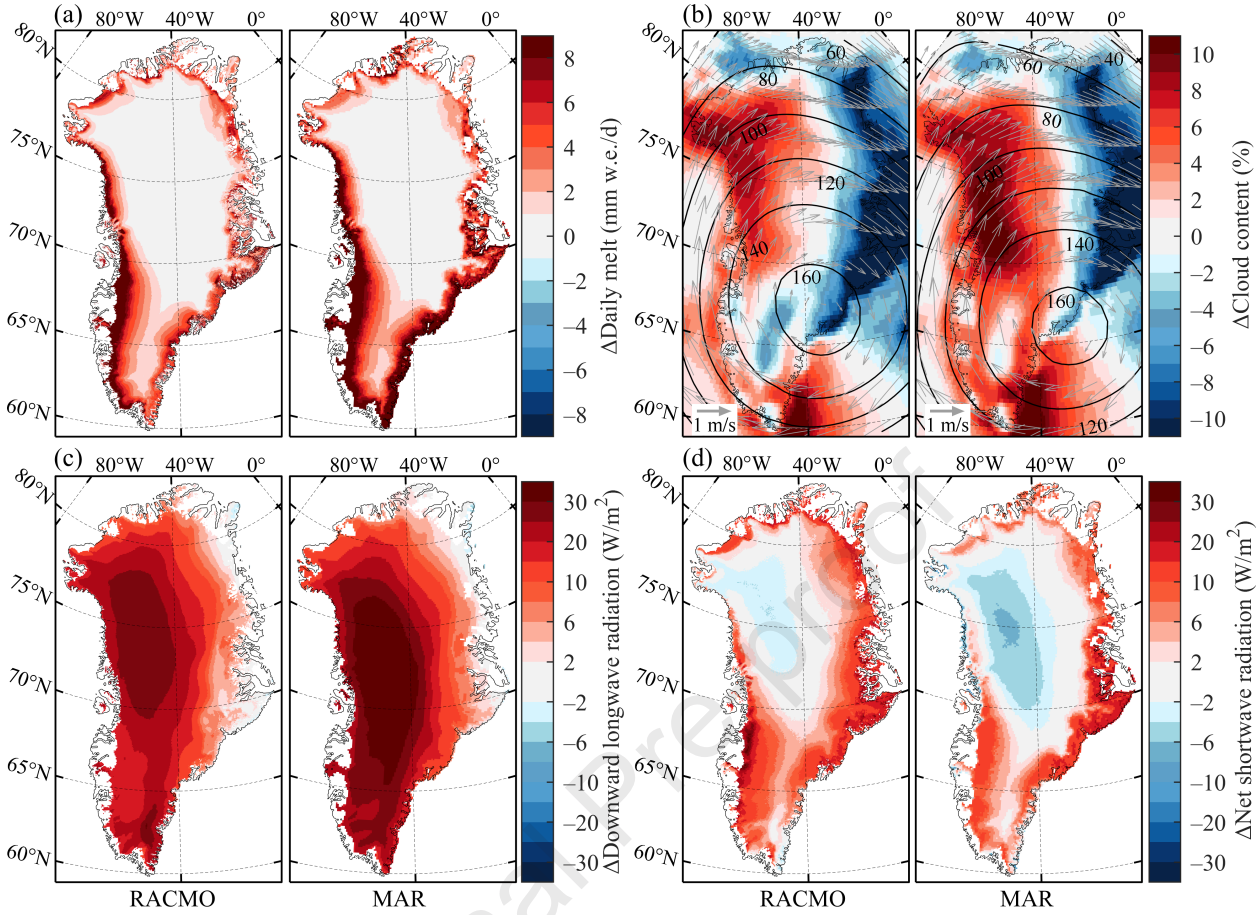

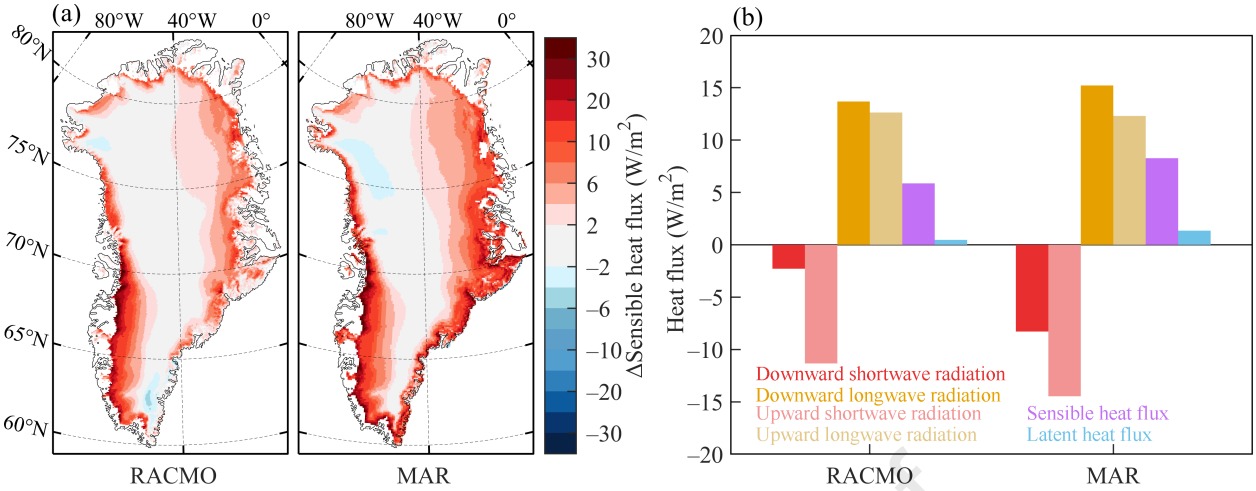

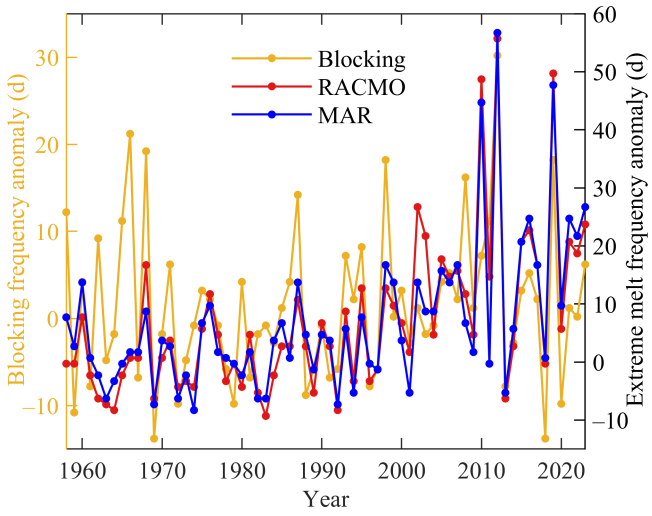

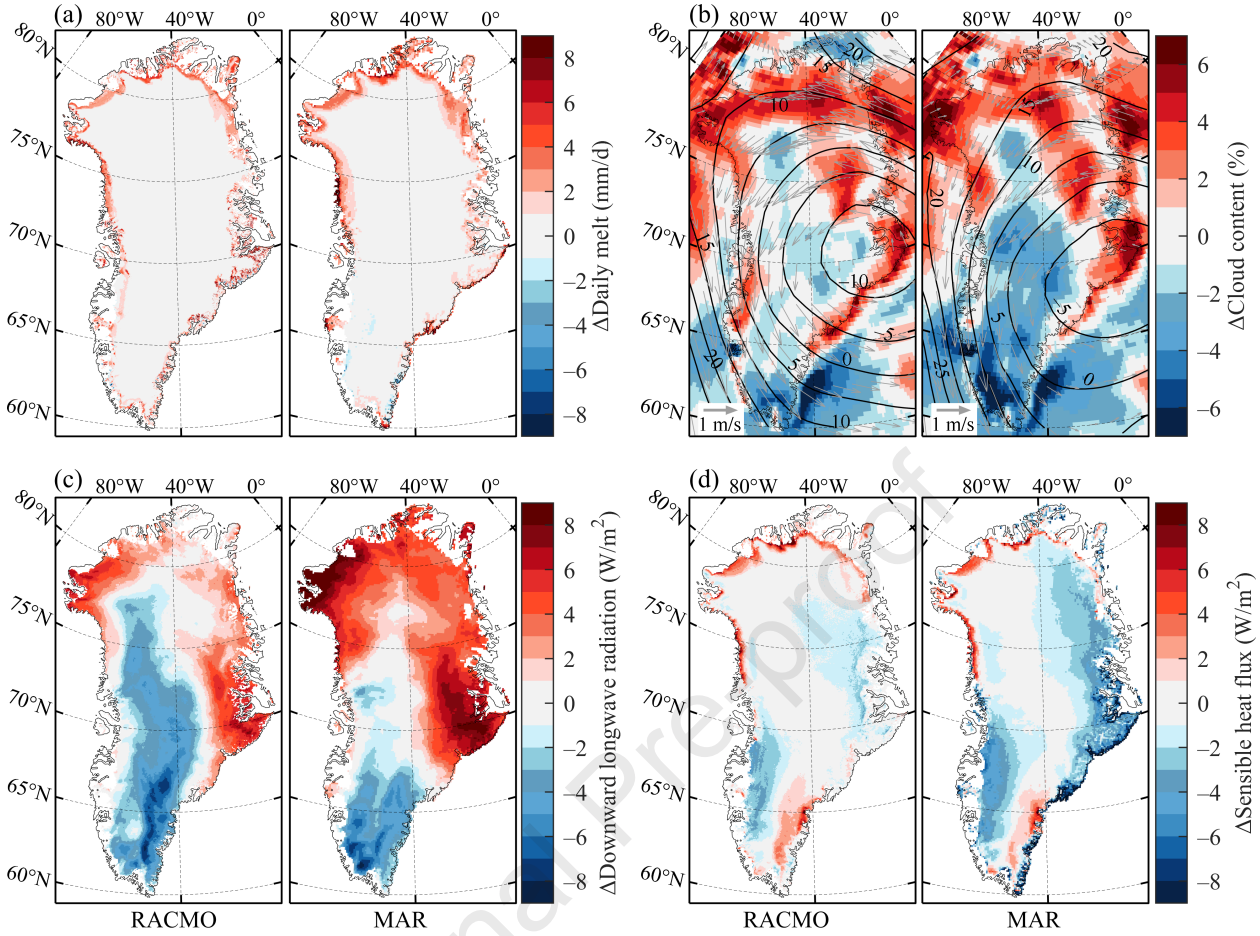

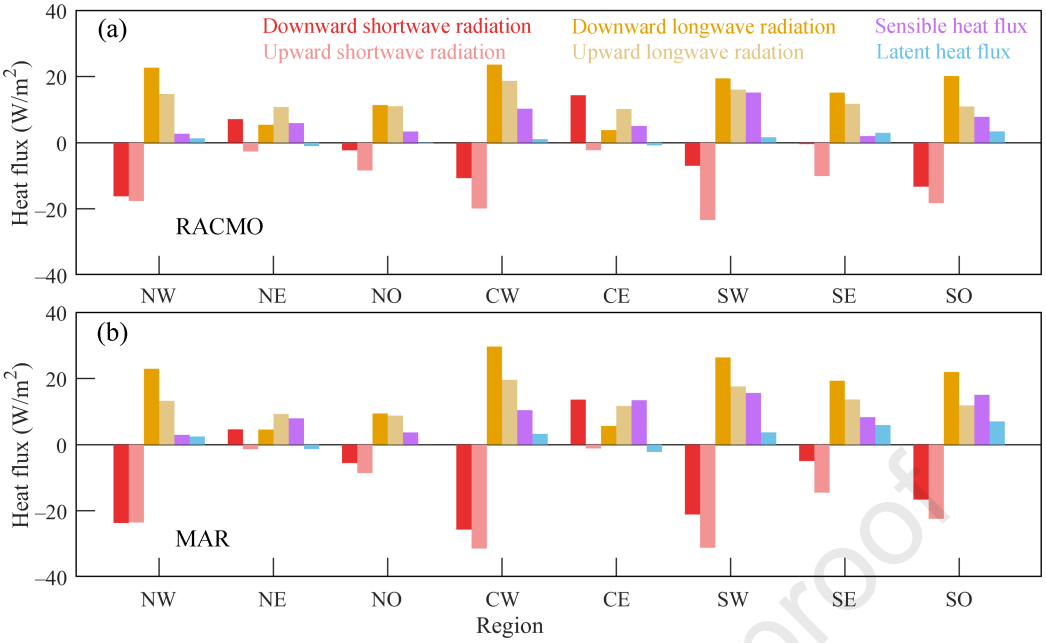

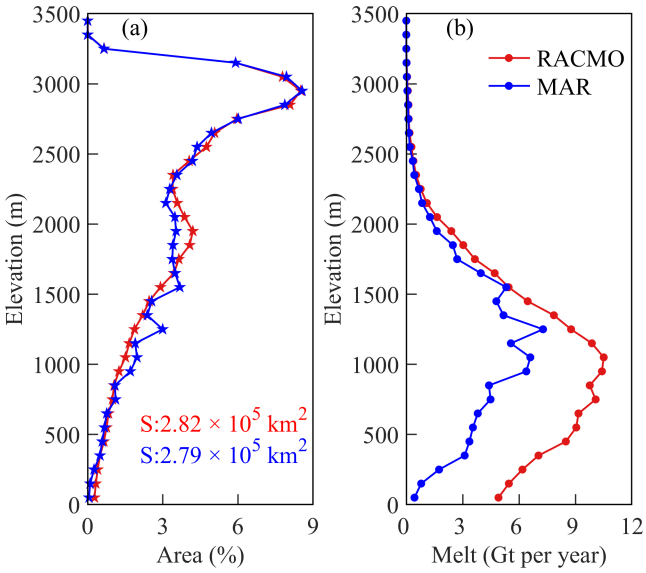

Declaration of competing interest

The authors declare no conflict of interest.